
Temperature-dependent optical properties of ϵ -Ga₂O₃ thin films

A PREPRINT

✉ **Takayuki Makino**
Far-IR R&D Center
University of Fukui
Fukui 910-8507, Japan
tmakino@u-fukui.ac.jp

Subaru Yusa
Department of Chemistry,
Tohoku University
Sendai 980-8578, Japan

✉ **Daichi Oka**
Department of Chemistry,
Tohoku University
Sendai 980-8578, Japan

✉ **Tomoteru Fukumura**
Department of Chemistry and WPI-AIMR
Tohoku University
Sendai 980-8577, Japan

November 1, 2023

ABSTRACT

We determined the complex dielectric functions of ϵ -Ga₂O₃ using optical transmittance and reflectance spectroscopies at temperatures from 10 K to room temperature. The measured dielectric-function spectra reveal distinct structures at bandgap energy. We fitted a model dielectric function based on the electronic energy-band structure to these experimental data. We analyzed the temperature dependence of the bandgap with a model based on phonon dispersion effects. One could explain it in terms of phonon-related parameters such as the optical phonon temperature. We compare phonon-related properties of ϵ -Ga₂O₃ with those of a large variety of element and binary semiconductors.

1 1. Introduction

Gallium oxide (Ga₂O₃) is an important wide-gap material from both fundamental and applied perspectives due to its potential applications such as power devices^{1,2)} and solar-blind UV photodetectors^{3,4)}. There are several polymorphs in this oxide.²⁾ The most stable phase among them is β -Ga₂O₃^{1,4)}. This polymorph has an indirect bandgap of 4.4–4.9 eV⁵⁾ and monoclinic crystalline symmetry.¹⁾ Despite intensive studies conducted on this polymorph^{5)–6)}, its complicated lattice structure became a bottleneck of further progress, such as the growth of heterojunctions with other materials^{7,8)}. On the other hand, corundum α -Ga₂O₃ has a relatively higher symmetry of the crystal^{9,10)}. And thus, an epitaxial thin film growth as a semiconductor device and its heteroepitaxial structures have been reported so far^{11,12)}. It is also possible to grow ϵ -Ga₂O₃^{13,14)}.

After pioneering work on the epitaxial thin film growth of ϵ -phase,¹⁵⁾ many research groups have reported various studies on this polymorph^{16,17)}. The X-ray diffraction studies initiated the long-standing debate on the crystalline structure of this polymorph^{17,18)}. Cora and coworkers¹⁸⁾ reported the ordered-oxygen-vacancy-site-induced reconstruction into the orthorhombic form^{19,20)}, sometimes referred to as the κ -phase. Attempts on the growth onto various substrates followed this seminal work^{21,22,23)}. More recently, a substrate-dependent properties assessment further developed systematic insight into this polymorph's potential possibilities^{24,25,26)}.

Furthermore, the recent reports on the high dielectric constants²⁷⁾ and the suitability of the heterostructure growth²⁴⁾ give rise to polymorph-dependent characteristic properties that may exhibit solely in this polymorph. However, further investigation of its basic material properties is necessary to realize its full potential. The temperature dependence of the optical properties is one of a semiconductor's fundamentally and technologically essential characteristics^{28,29)}. One may expect that this investigation offers more profound insights into various aspects such as electron-phonon interaction, thermal properties, and phononic properties. So far, spectroscopic measurements have been done only

at room temperature^{23),27)}. In other words, no one has conducted this in the cryogenic temperature range for this polymorph to the best of our knowledge.

In this paper, we report the temperature dependence of the optical properties of ϵ -Ga₂O₃ thin films. We emphasize the interpretation of the temperature dependence of the bandgap energies from the viewpoint of the electron-phonon interaction particularly^{30),31)}. Finally, we compare the phononic properties of Ga₂O₃ with those of other materials.

2 Experimental methods

ϵ -Ga₂O₃ epitaxial thin films were grown at 570 °C on sapphire (0001) substrates^{27),32)}. Our adopted technique is mist chemical vapor deposition (CVD). This technique is a facile solution process at atmospheric pressure.¹²⁾ In its growth, one used an aqueous solution of 0.025 M gallium acetylacetonate and 0.05 M hydrochloric acid as a precursor. We nebulized the precursor solution using ultrasonic transducers. We transferred it to the substrates in a tubular furnace with nitrogen gas flow from the carrier and dilution ports at 3.0 L/min and 0.5 L/min, respectively. The crystalline structure of this phase and its structural properties can find themselves in Figs. 1 and 2 of Ref. 27, indicating the high crystalline quality of our films.

We measured the transmission (T) and reflection (R) spectra at a beamline of the UVSOR facility in the Institute of Molecular Science, Japan. One attached the samples on a cold finger of the refrigerator for the temperature-dependent measurements. We do not plot the transmission or reflection spectrum but the dielectric functions because of the intimacy with various electronic-structure-related quantities. First, we modeled our Ga₂O₃/sapphire system to determine the real and imaginary components of dielectric constants.³³⁾ We used a homemade multilayer analysis program to do this task. The complicated conversion is necessary between optical and dielectric functions because these are related to both the film and substrate parameters. In addition, the equations giving the reflectivity and transmission explicitly in terms of the dielectric constants of the film and the substrate are very complicated and have multiple solutions. An iterative Newton-Raphson method determines the dielectric constants by minimizing an error function composed of calculated and experimental values. Denton and coworkers³³⁾ showed that using expressions for $(1 \pm R)/T$ rather than the explicit formulae for the reflectivity and the transmission simplifies the problem and eases the computing burden. In this way, we found those components that best explain the experimental data. We performed this analysis sequentially for each wavelength to obtain the dielectric functions.

3 Results and discussions

3.1 Relationship with electronic structures and model dielectric function analysis

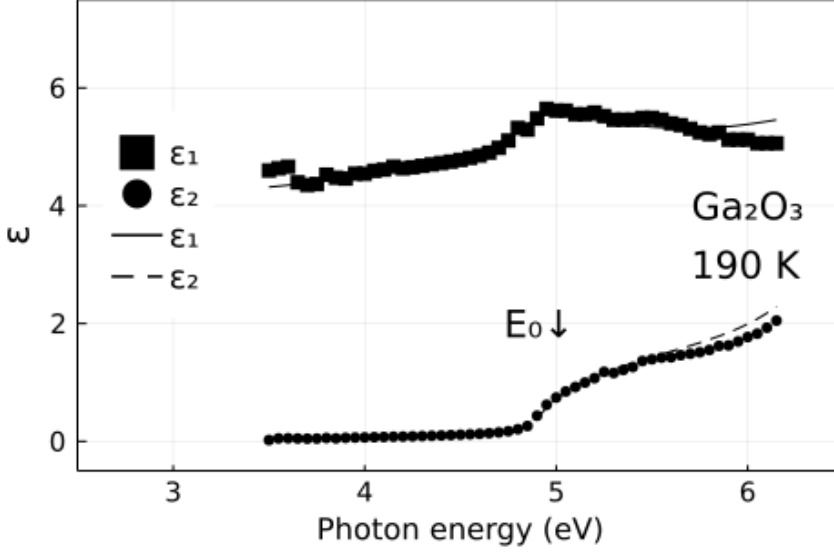
For purposes of discussion, we consider the band structures of Ga₂O₃^{34),35)}. The κ related band diagram can find itself in Fig. 2 of Ref. 35. In many semiconductors, optical transitions related to the fundamental absorption edge associate with three-dimensional direct M_0 -type critical points^{36),37)}. Because there has been no report on strong anisotropy in the valence and conduction bands as far as Ga₂O₃ is concerned^{34),35),38)}. Thus we assign the fundamental absorption edge to M_0 transitions from the highest valence band to the lowest conduction band at the Γ point. The corresponding optical transition is labeled E_0 . As later described, we did not account for the spin-orbit split component. To account for the experimental curves over the entire photon energy range, it was also necessary to include the influence of the E_1 transitions.³⁵⁾ Furthmüller and coworkers³⁴⁾ theoretically reported a higher-lying-gap-related structure in the dielectric functions in the ϵ -phase at *ca.* 5 eV. Because the calculation based on the density functional theory underestimates the bandgap energies, we assign this to the E_1 gap at *ca.* 6.8 eV by considering this redshift effect (approximately 2 eV). The energetic position is even higher than the measured photon energy range (6.2 eV). This transition is labeled E_1 in this work.

We describe here the model dielectric functions. Transitions involving these energy bands are responsible for all the features in the dielectric functions. In a model that we have employed, one approximates the dielectric function as a sum of several components, each of which is an explicit function of energy. The dielectric function represents a contribution from the neighborhood of a critical point in the joint density of states. We use the following M_0 -type dielectric functions for the E_0 transition. This transition occurs at a photon energy of 4.89 eV at 190 K. Assuming the bands are parabolic, we obtain the contribution of this gap to the dielectric function^{36),37)}:

$$\epsilon(\hbar\omega) = \frac{A_0}{E_0^{1.5}} \left[\chi_0^{-2} \left\{ 2 - (1 + \chi_0)^{0.5} - (1 - \chi_0)^{0.5} \right\} \right], \quad \# (1)$$

With

Figure 1: Real (squares) and imaginary (circles) parts of the dielectric functions of Ga₂O₃ thin-film taken at 190 K. The symbols are the experimental data. The lines are calculated for real (solid) and imaginary (dashed) parts using Eqs. (1)-(3), and $\epsilon_{1\infty} = 2.5$.



$$\chi_0 = \frac{\hbar\omega + i\Gamma}{E_0} \quad (2)$$

Values of A_0 and Γ_0 in Eqs. (1) and (2) correspond to the strength and broadening parameters in this optical transition.

We next describe the E_1 feature. We labeled a structure found in the optical spectra in the region higher than E_0 as E_1 (~ 6.8 eV). The E_1 peak is difficult to analyze as it does not correspond to single, well-defined critical points. Thus, we have characterized the E_1 structure (not observed) as a damped harmonic oscillator^{36,37}:

$$\epsilon(\hbar\omega) = \frac{A_1}{1 - \chi_3^2 - i\Gamma_1\chi_1} \quad (3)$$

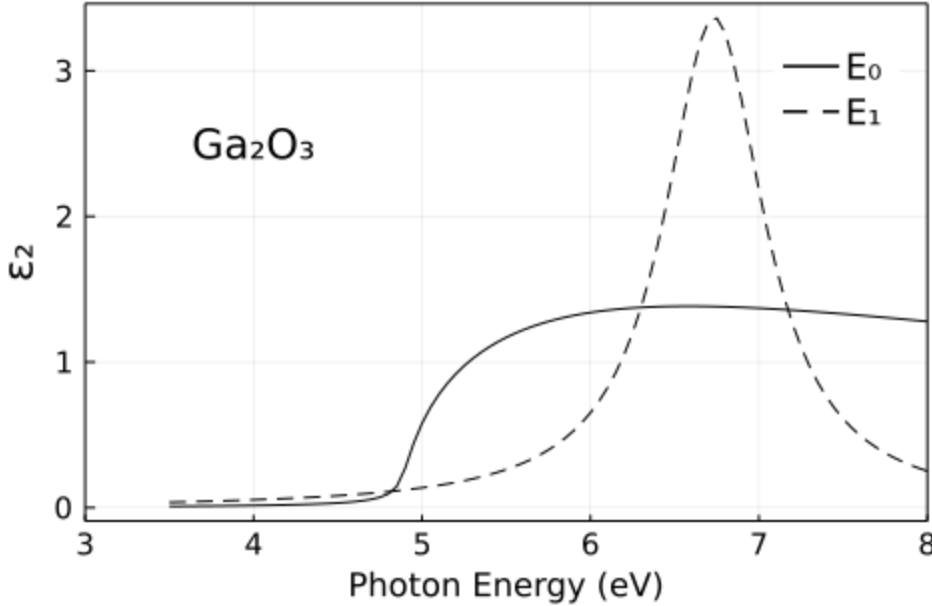
with $\chi_1 = E/E_1$ Where A_1 is a *dimensionless* strength parameter. The quantity Γ_1 stands for a *dimensionless* broadening parameter.

We then describe the total dielectric function. The whole dielectric function was found by summing the expressions given previously. We used The parameters such as A_0 and A_1 as adjustable constants to calculate the dielectric functions. If we wish to obtain, for example, the imaginary parts (ϵ_2), we can take the imaginary part of Eqs. (1) and (3). A constant, $\epsilon_{1\infty}$ was added to the real part of the dielectric constant (ϵ_1) to account for the vacuum plus contributions from higher-lying energy gaps^{36,37,39}. The model presented above can fit the experimental dispersion of dielectric functions over the entire range of the measurements.

Square and circle symbols in Fig. 1 show the real and imaginary parts of the dielectric functions of Ga₂O₃. The measurement temperature is 190 K. One obtained these data from the analysis of the experimental data on T and R . An arrow denotes the value of the interband transition E_0 . The solid and dashed lines in Fig. 1 correspond to the results of the least-squares fit. The model functions are Eqs. (1) - (3). There is reasonable agreement between the experiment and the results of fit. We evaluate E_0 , A_0 , and Γ_0 to be 4.89 eV, 47 eV^{3/2}, and 45 meV, respectively. We can quickly determine an initial guess of parameterization for the energy E_0 because this energy corresponds to the onset in the imaginary dielectric function (ϵ_2). Even after the regression analysis, this remained almost unchanged. The obtained strength parameter value is reasonable because it often ranges in tens of eV^{3/2} in many semiconductors^{36,37}. An empirical rule tells us that the broadening parameter tends to be somewhat greater than the corresponding thermal energy (*ca.* 20 meV for 190 K), which is also valid for this case.

Displayed in Figs. 2 and 3 are the individual contributions to the real (ϵ_1) and imaginary (ϵ_2) parts of the complex dielectric functions, respectively, of the two transitions. The related equations are for the three-dimensional M_0 critical

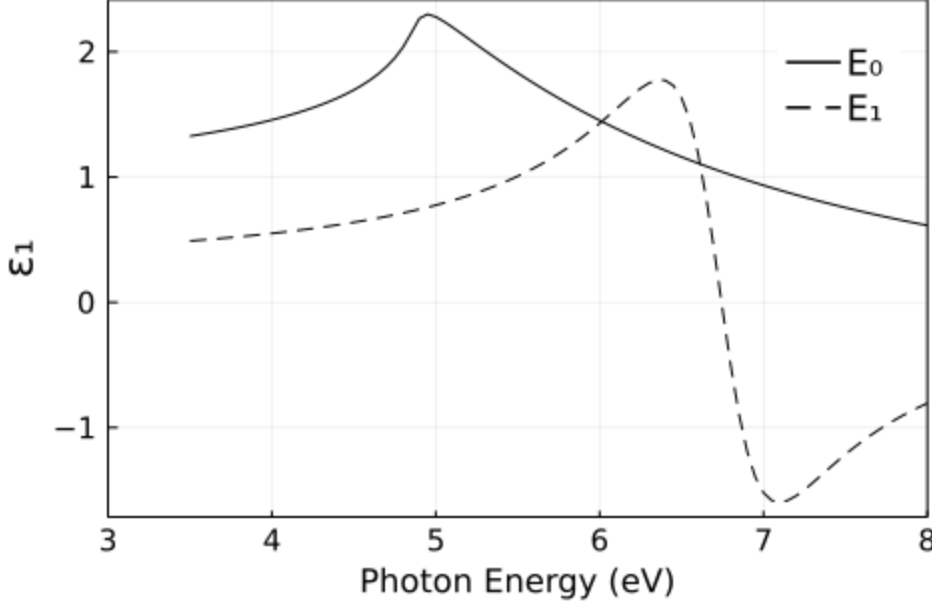
Figure 2: Individual contribution to the imaginary part of the dielectric function of the two energy gaps for Ga₂O₃. They are obtained from Eqs. (1) and (2) for the M_0 contribution, and from Eq. (3) for the E_1 -gap contribution.



point and the E_1 resonances. We evaluate $\epsilon_{1\infty}$ to be 2.5. Adachi and coworkers analyzed the dielectric function to determine this value for many semiconductors^{36),37)}. In many cases, this value is often slightly larger than unity. The value obtained in this work is significantly greater than that in other semiconductors. This observation is consistent with the fact that the ϵ -phase has a higher static dielectric constant than the different phases of Ga₂O₃ or many semiconductors. Readers might think the influence of strain disturbs the precise evaluation of the bandgap energy. Indeed, there is strain between the substrate and the thin film due to the lattice mismatch. We can safely rule out that apprehension. Understanding the following facts can convince of its validity. In general, only very high-precision spectroscopy can detect very tiny energy shifts induced by externally applied stress. Due to the relaxation, the lattice-mismatch-induced strain is considerably smaller than the strain usually used in external stress experiments. Therefore, we can neglect its influence on the bandgap energy. Likewise, we argue the effect of inhomogeneity on the bandgap energy. We know well that the inhomogeneity induces an exponential tail to the onset in the imaginary dielectric function. We do not observe, however, such a tail state. Therefore, we can safely rule out that possibility. The direct gap does not exhibit a well-defined excitonic structure either. This absence is probably consistent with the high-dielectric nature of this thin film.²⁷⁾ According to Goñi and coworkers,⁴⁰⁾ the binding energy of the exciton includes the terms of the static dielectric constant and the effective masses of the relevant electrons and holes. In other words, a higher dielectric constant leads to smaller binding energy, while higher effective mass gives rise to the larger binding energy. We know that the ϵ -phase of Ga₂O₃ has a relatively high static dielectric constant.²⁷⁾ There is no theoretical report suggesting the large effective mass of the electron and hole. In general, the layer-type crystalline structures tend to have large effective masses, which is not the case here. The spin-orbit splitting in the valence band is frequently present in many semiconductors with long search history. Our experimental results do not find themselves the splitting-related distinct structures. Theoretical studies on the electronic structures have not discussed the splitting in this phase. Even worse, an enlarged view of the band diagram near the valence band is not available. Therefore, theoretical works cannot offer a basis for this splitting effect to analyze our experimental data. Nevertheless, a weak inflection point observed near 5.5 eV in the imaginary dielectric function (ϵ_2) might be reminiscent of this splitting. The difference from the fundamental bandgap energy amounts to 0.5 or 0.6 eV, consistent with those found in many semiconductors.³⁹⁾ We do not, however, consider this splitting here for the abovementioned reasons. We evaluate E_1 , A_1 , and Γ_1 to be 6.74 eV, 0.36, and 110, respectively. The E_1 transition parametrization is complicated because this is outside of the measured energy range. The related parameters are mutually interdependent.

3.2 Fitting with Pässler's model

Closed circles in Fig. 4 show the temperature dependence of the bandgap energy (TDBGE) in Ga₂O₃. One confirms that the bandgap energy (E_0) is a monotonically decreasing function of temperature (T).²⁸⁾ Because the repulsion between

Figure 3: Individual contribution to the imaginary part of the dielectric function of the two energy gaps for Ga₂O₃.

electrons decides the bandgap energy, thermal expansion of the crystal volume will result in the bandgap shrinkage. As earlier mentioned, the interface-strain-effect-induced energetic shift is negligible in our case. The external application of stress gives rise to a change, a typical magnitude of which is amounted much smaller than the temperature-induced energetic shift observed here. The interface strain is several orders of magnitude smaller than the typical strain values of these external stress experiments.

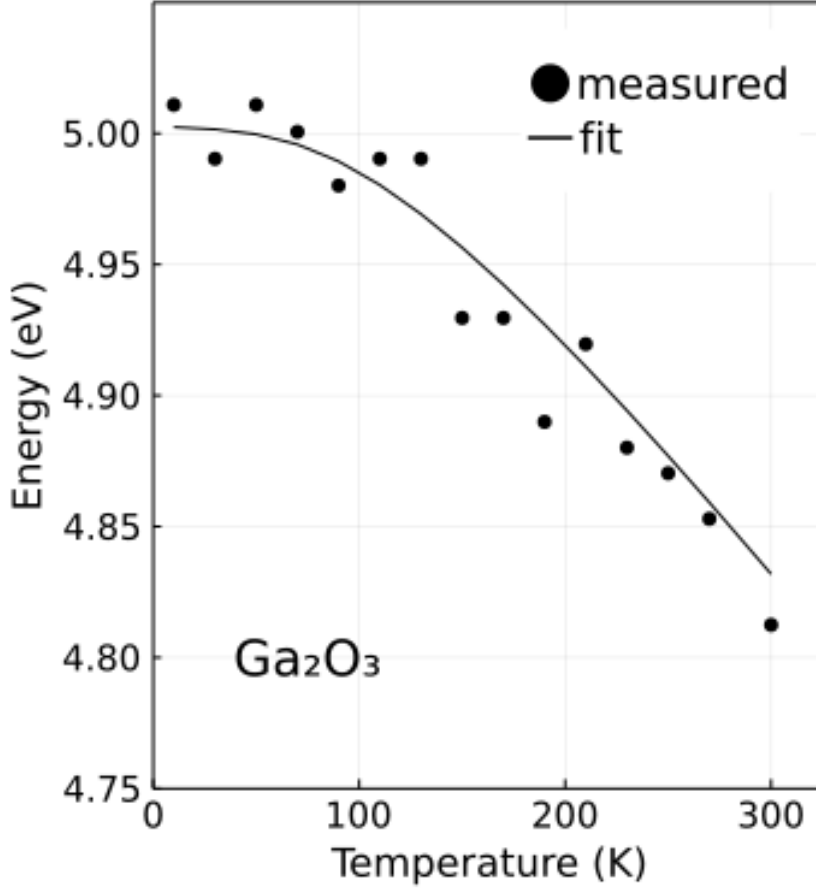
Usually, one analyzes the TDBG using Varshni's model.⁴¹⁾ This model assumes an unreasonably large phonon width. Therefore, the difficulty is often associated with the interpretation of the fitting parameters. Instead of that model, we use Pässler's model to fit the experimental data^{29),30)}. Here the corresponding equation as a function of temperature can be expressed:³¹⁾

$$E_0(T) = E_0(0) - \alpha\Theta \frac{(1 - 3\Delta^2)}{\exp(\frac{\Theta}{T}) - 1} + \frac{3\Delta^2}{2} \left(\sqrt[6]{1 + \frac{\pi^2}{3(1 + \Delta^2)} \left(\frac{2T}{\Theta}\right)^2 + \frac{3\Delta^2 - 1}{4} \left(\frac{2T}{\Theta}\right)^3 + \frac{8}{3} \left(\frac{2T}{\Theta}\right)^4 + \left(\frac{2T}{\Theta}\right)^6} - 1 \right) \quad (4)$$

We here explain the meaning of the related symbols: α is the high-temperature limit of a slope, Δ is a phonon-width-related parameter, Θ an effective phonon temperature, and E_0 a fundamental gap's energy, respectively. As later discussed in detail, we fixed Δ ($= 0.35$) and Θ ($= 343$ K) parameters as decided from PDOS (phonon density-of-states) spectrum. The determined values for the abovementioned parameters in Ga₂O₃ are as follows: $\alpha = 1.0 \times 10^{-3}$ eV/K, $E_0(0) = 5.00$ eV, respectively. A solid trace in Fig. 4 corresponds to the fit for the case that the width-related parameter (Δ) is equal to 0.35. The calculated result agreed reasonably with the experimental monotonical behavior. According to Pässler^{29),30)}, a critical temperature range certainly exists where the curvature in the temperature-dependent energy gap curve sensitively depends on the materials' properties. One can calculate this temperature range by using the effective phonon temperature and dimensionless phonon dispersion coefficient. The definitions of these two quantities can find themselves later in detail. The critical temperatures range from 750 K to 1160 K for this polymorph. Our measurement indeed covered this temperature range, enabling us to evaluate the materials' parameters. Change of the polymorph gives rise to the changes in this temperature range and the curvature in the temperature-dependent energy gap curve. Such a polymorph-dependent comparative study may be intriguing, which is albeit beyond the scope of this work.

We describe how to determine the effective phonon temperature (Θ) from the PDOS lineshape. We assume that this temperature (Θ) is equal to an averaged phonon temperature (Θ_p). That is: $\Theta_p = (\Theta_U + \Theta_L)/2$. Here, Θ_L (Θ_U) stands for a temperature corresponding to energetically-lower (-upper) acoustic (optical) phonon's peak frequency in the theoretically-calculated ϵ -phase PDOS.⁴²⁾ For the conversion from the peak frequency to the temperature, we adopted

Figure 4: Temperature dependences of direct bandgap E_0 observed in Ga₂O₃ (circles). A curve (solid) corresponds to a numerical fit to the experimental data field using Eq. (4) with phonon dispersion-related parameters.



Boltzmann's constant (k_B). The TDBGE analysis uses the phonon temperature (Θ_p) because we know empirically that the effective phonon temperature (Θ) is almost equal to the effective phonon temperature (Θ_p).

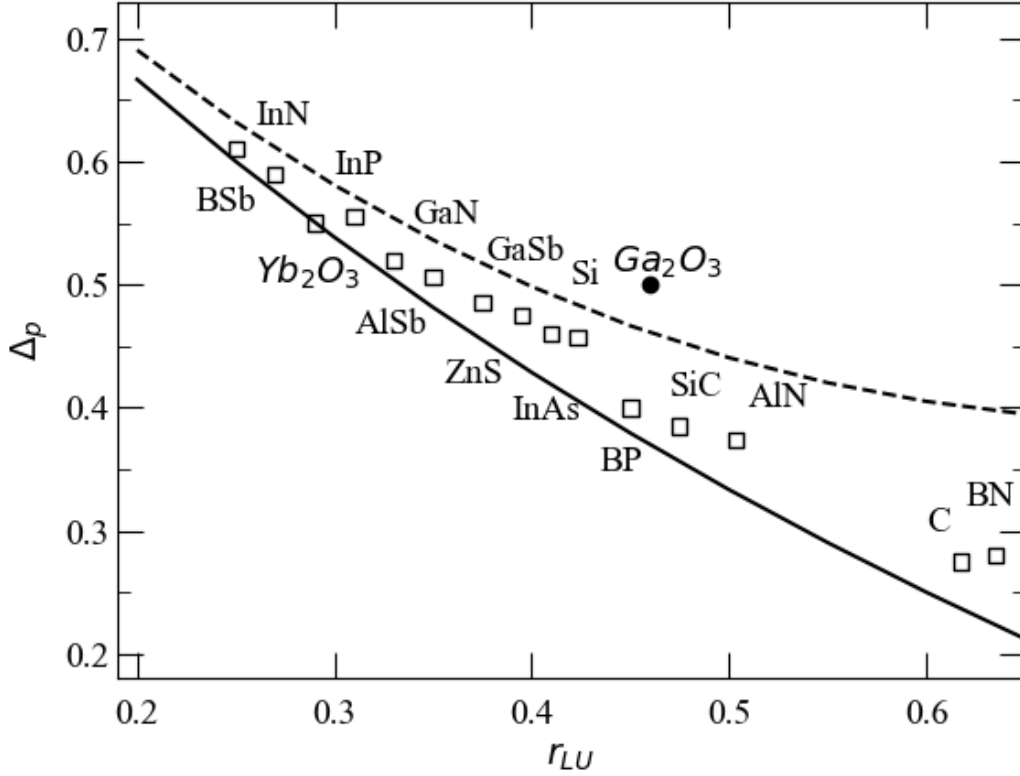
Next, let us define a dimensionless dispersion coefficient related to the averaged variance in the following:

$$\Delta_P = \frac{\sqrt{V_P - \mu_P^2}}{\mu_P} \quad (5)$$

Here, V_p stands for the averaged variance between those of the acoustic and the optical phonons. μ_p means averaged phonon frequency ($\mu_p = \Theta_p / k_B$). We evaluate the coefficient Δ_P of Ga₂O₃ to be *ca.* 0.50. An empirical rule established from a database of a variety of materials tells us that the width-related parameter (Δ) tends to be approximately 70% of Δ_P .⁴³⁾ We used these values for the above analysis, as shown with the solid line in Fig. 4.

We comment about the parameters used in the bandgap energy fit [Eq. (4)] to the experimental data. Because the visual inspection of the experimental data enables us to determine $E_0(0)$ we can concentrate on evaluating the slope parameter (α) with the fitting. We could quickly determine an initial guess of parameterization for the slope (α) because this may correspond to the energy difference between $T = 10$ K and room temperature. After the regression analysis, the deviation from the initial guess is in a reasonable range. Reducing the number of fitting parameters is an advantage. Therefore, the significance of the phonon-property-related discussion is the reduction of the ambiguity in the analysis.⁵¹⁾

Figure 5: Visualization (open squares and a closed circle) of the roughly monotonic decrease of the magnitudes of dimensionless dispersion coefficients Δ_p , with increasing the relative phonon temperature, r_{LU} . Observing that the partial dispersion coefficients for the lower and upper sections are limited to the intervals for almost all materials readily establishes the lower and upper boundaries for this ratio.



3.3 3.3 Discussions

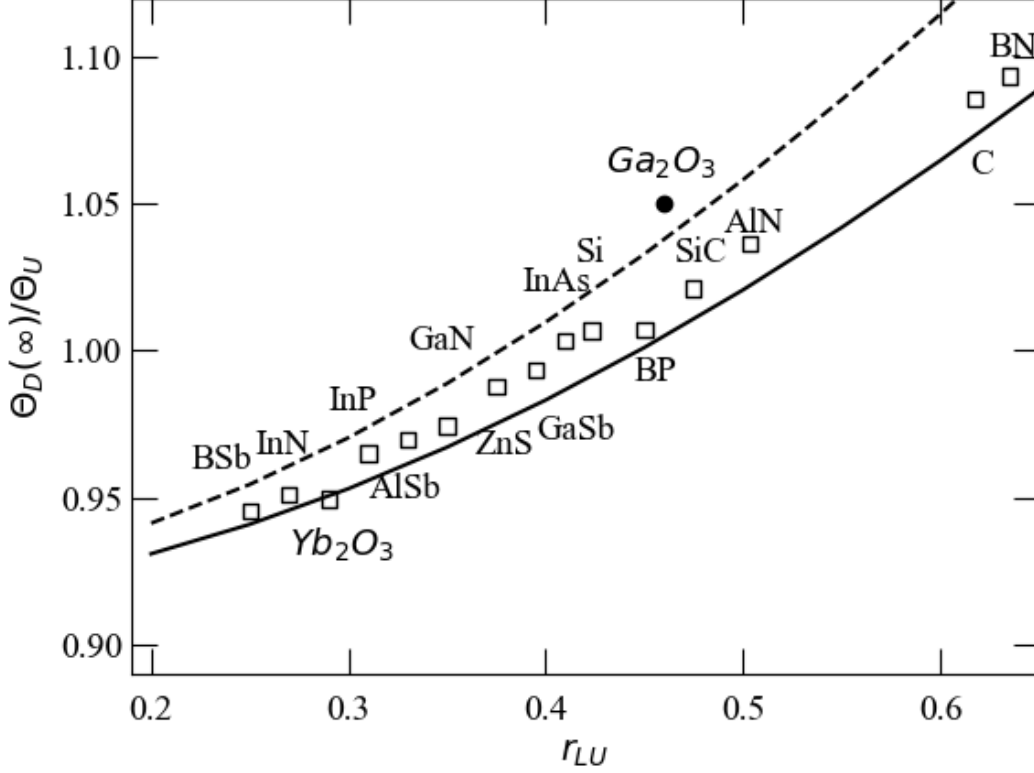
In the remainder, we compare the dimensionless dispersion coefficient and Debye's temperature with various semiconductors^{43,44}. First, let us define the following quantity: $r_{LU} = \frac{\Theta_L}{\Theta_U}$. We call it a relative phonon temperature. Discussion in terms of this quantity gives rise to better insight. The relative phonon temperature (r_{LU}) of Ga₂O₃ is 0.46. This value is similar to those in SiC or AlN widegap semiconductors. Open circles and a closed circle in Fig. 5 show the magnitude of dimensionless dispersion coefficients (Δ_p) as a function of the relative phonon temperature (r_{LU}). We calculated the lower and upper zone boundaries for Δ_p according to Ref. 44. Solid and dashed traces, respectively, represent these. We used the following equation to draw these functions:

$$\frac{1 - r_{LU}}{1 + r_{LU}} < \Delta_p < \frac{\sqrt{(1 - r_{LU})^2 + \frac{2}{3}r_{LU}^2 + 0.02}}{1 + r_{LU}} \quad (6)$$

The practical limitations of the partial dispersion coefficients of optical and acoustic phonons determine these boundaries. It is a well-known fact that many semiconductor materials' phonons exist within the zones (limits) mentioned above^{44,45}. As shown in Fig. 5, we observe that a datum of Ga₂O₃ (emphasized using a closed circle) slightly deviates from the upper boundary. This deviation may be related to the high static dielectric constant of ϵ -Ga₂O₃²⁷. Further studies are necessary to clarify this issue.

Figure 6 shows the relative phonon temperature (r_{LU}) dependence of a normalized Debye temperature $\Theta_D(\infty)/\Theta_U$ (open circles and a closed circle). Here, $\Theta_D(\infty)$ stands for a limiting Debye temperature. The definition of the limiting Debye temperature is as follows:

Figure 6: Open squares and a closed circle show the magnitudes of the ratio $\frac{\Theta_D(\infty)}{\Theta_U}$ plotted against the relative phonon temperature. Here, $\Theta_D(\infty)$ stands for the limiting Debye temperatures.



$$\Theta_D(\infty) = k_B^{-1} \sqrt{\frac{5}{3}} V_P. \quad (7)$$

We calculated the normalized Debye temperature ($\Theta_D(\infty)/\Theta_U$) for ϵ -Ga₂O₃ as 1.05. As has been already explained, the practical limits of the phonon dispersion decide the upper and lower regions. The resulting equations are as follows:

$$\sqrt{\frac{5}{6}} (1 + r_{LU}^2) < \frac{\Theta_D(\infty)}{\Theta_U} < \sqrt{\frac{5}{6}} \left(1.01 + \frac{4}{3} r_{LU}^2 \right) \quad (8)$$

4 Conclusion

We assessed the temperature dependence of the optical properties for ϵ -Ga₂O₃ thin films. We have been able to extract several important material parameters. We interpreted the TDBG model along a model based on the electron-phonon interaction. We compared the phonon-related parameters of Ga₂O₃, such as the dimensionless dispersion coefficient of phonons (Δ) and the normalized Debye temperature ($\Theta_D(\infty)/\Theta_U$) with those of many semiconductors.

5 Acknowledgments

This work was in part conducted in a beamline of the UVSOR facility, Institute for Molecular Science, Okazaki, Japan. We also acknowledge the partial financial support of this work from JSPS KAKENHI Grant Number 19K05303. In addition, we acknowledge technical assistance from T. Asai, T. Nishiwaki, and T. Takeuchi.

6 References

- 1) M. Higashiwaki, H. Murakami, Y. Kumagai and A. Kuramata, *Jpn. J. Appl. Phys.* **55**, 1202A1 (2016).
- 2) Y.-W. Huan, S.-M. Sun, C.-J. Gu, W.-J. Liu, S.-J. Ding, H.-Y. Yu, C.-T. Xia and D. W. Zhang, *Nanoscale Res. Lett.* **13**, 246 (2018).
- 3) S. J. Pearton, J. Yang, P. H. Cary, F. Ren, J. Kim, M. J. Tadjer and M. A. Mastro, *Appl. Phys. Rev.* **5**, 011301 (2018).
- 4) Z. Galazka, *Semicond. Sci. & Technol.* **33**, 113001 (2018).
- 5) E. G. Villora, K. Shimamura, Y. Yoshikawa, K. Aoki and N. Ichinose, *J. Cryst. Growth* **270**, 420 (2004).
- 6) H. Aida, K. Nishiguchi, H. Takeda, N. Aota, K. Sunakawa and Y. Yaguchi, *Jpn. J. Appl. Phys.* **47**, 8506 (2008).
- 7) J. /AAhman, G. Svensson and J. Albertsson, *Acta Crystallog. C* **52**, 1336 (1996).
- 8) S. Geller, *J. Chem. Phys.* **33**, 676 (1960).
- 9) D. Shinohara and S. Fujita, *Jpn. J. Appl. Phys.* **47**, 7311 (2008).
- 10) K. Kaneko, I. Takeya, S. Komori and S. Fujita, *J. Appl. Phys.* **113**, 233901 (2013).
- 11) K. Kaneko, Y. Ito, T. Uchida and S. Fujita, *Appl. Phys. Express* **8**, 095503 (2015).
- 12) S. Fujita, M. Oda, K. Kaneko and T. Hitora, *Jpn. J. Appl. Phys.* **55**, 1202A3 (2016).
- 13) R. Roy, V. G. Hill and E. F. Osborn, *J. Am. Chem. Soc.* **74**, 719 (1952).
- 14) H. Y. Playford, A. C. Hannon, E. R. Barney and R. I. Walton, *Chem. European J.* **19**, 2803 (2013).
- 15) Y. Oshima, E. G. Villora, Y. Matsushita, S. Yamamoto and K. Shimamura, *J. Appl. Phys.* **118**, 085301 (2015).
- 16) X. Xia, Y. Chen, Q. Feng, H. Liang, P. Tao, M. Xu and G. Du, *Appl. Phys. Lett.* **108**, 202103 (2016).
- 17) F. Mezzadri, G. Calestani, F. Boschi, D. Delmonte, M. Bosi and R. Fornari, *Inorganic Chem.* **55**, 12079 (2016).
- 18) I. Cora, F. Mezzadri, F. Boschi, M. Bosi, M. Caplovicova, G. Calestani, I. Dodony, B. Pecz and R. Fornari, *CrystEngComm* **19**, 1509 (2017).
- 19) Y. Zhuo, Z. Chen, W. Tu, X. Ma, Y. Pei and G. Wang, *Appl. Surf. Sci.* **420**, 802 (2017).
- 20) D. Tahara, H. Nishinaka, S. Morimoto and M. Yoshimoto, *Jpn. J. Appl. Phys.* **56**, 078004 (2017).
- 21) H. Sun, K.-H. Li, C. G. T. Castanedo, S. Okur, G. S. Tompa, T. Salagaj, S. Lopatin, A. Genovese and X. Li, *Cryst. Growth & Design* **18**, 2370 (2018).
- 22) D. Tahara, H. Nishinaka, S. Morimoto and M. Yoshimoto, *Appl. Phys. Lett.* **112**, 152102 (2018).
- 23) H. Nishinaka, N. Miyauchi, D. Tahara, S. Morimoto and M. Yoshimoto, *CrystEngComm* **20**, 1882 (2018).
- 24) V. Gottschalch, S. Merker, S. Blaurock, M. Kneiss, U. Teschner, M. Grundmann and H. Krautscheid, *J. Cryst. Growth* **510**, 76 (2019).
- 25) M. Kneiss, A. Hassa, D. Splith, C. Sturm, H. von Wenckstern, T. Schultz, N. Koch, M. Lorenz and M. Grundmann, *APL Materials* **7**, 022516 (2019).
- 26) Y. Xu, J.-H. Park, Z. Yao, C. Wolverton, M. Razeghi, J. Wu and V. P. Dravid, *ACS Appl. Mater. & Interf.* **11**, 5536 (2019).
- 27) S. Yusa, D. Oka and T. Fukumura, *CrystEngComm* **22**, 381 (2020).
- 28) H. Pettersson, R. Pässler, F. Blaschta and H. G. Grimmeiss, *J. Appl. Phys.* **80**, 5312 (1996).
- 29) R. Pässler, *J. Appl. Phys.* **83**, 3356 (1998).
- 30) R. Pässler, *Phys. Rev. B* **66**, 085201 (2002).
- 31) R. Pässler, *Phys. Status Solidi (b)* **236**, 710 (2003).
- 32) D. Oka, S. Yusa, K. Kimura, A. K. R. Ang, N. Hapoo, K. Hayashi and T. Fukumura, *Jpn. J. Appl. Phys.* **59**, 010601 (2019).
- 33) R. E. Denton, R. D. Campbell and S. G. Tomlin, *J. Phys. D* **5**, 852 (1972).

- 34) J. Furthmüller and F. Bechstedt, Phys. Rev. B **93**, 115204 (2016).
- 35) J. Kim, D. Tahara, Y. Miura and B. G. Kim, Appl. Phys. Express **11**, 061101 (2018).
- 36) S. Adachi, Phys. Rev. B **35**, 7454 (1987).
- 37) S. Adachi, J. Appl. Phys. **66**, 813 (1989).
- 38) H. He, R. Orlando, M. A. Blanco, R. Pandey, E. Amzallag, I. Baraille and M. Rérat, Phys. Rev. B **74**, 195123 (2006).
- 39) S. Adachi and T. Taguchi, Phys. Rev. B **43**, 9569 (1991).
- 40) A. R. Goñi, K. Syassen, Y. Zhang, K. Ploog, A. Cantarero and A. Cros, Phys. Rev. B **45**, 6809 (1992).
- 41) Y. P. Varshni, Physica (Utrecht) **34**, 149 (1967).
- 42) S. Yoshioka, H. Hayashi, A. Kuwabara, F. Oba, K. Matsunaga and I. Tanaka, J. Phys.: Cond. Matter **19**, 346211 (2007).
- 43) R. Pässler, Phys. Status Solidi (b) **243**, 2719 (2006).
- 44) R. Pässler, J. Appl. Phys. **101**, 093513 (2007).
- 45) T. Makino, T. Asai, T. Takeuchi, K. Kaminaga, D. Oka and T. Fukumura, Jpn. J. Appl. Phys. **59**, SCCB13 (2020).